

Topology of the Magnetic Domains of a Co/Pt Multilayer
with 16Å Cobalt Layers

Matthew Healey

A capstone report submitted to the faculty of
Brigham Young University
In partial fulfillment of the requirements for the degree of
Bachelor of Science

Dr. Karine Chesnel, Advisor

Department of Physics and Astronomy

Brigham Young University

June 10, 2016

© 2016 Matthew Healey
All Rights Reserved

ABSTRACT

Topology of the Magnetic Domains of a Co/Pt Multilayer with 16Å Cobalt Layers

Matthew Healey
Department of Physics and Astronomy
Bachelor of Science

It was recently established, through MFM microscopy, that the magnetic domain topology in Co/Pt (cobalt-platinum) multilayered thin films can be influenced by the magnetic history of the material (i.e. the magnetic path which the material has been exposed to). Particularly, it appears that the domain topology at remanence drastically depends on the magnitude of the field previously applied perpendicular to the material. A maximum density of domains is obtained after a magnetic field of appropriate strength has been applied. We are expanding this study by showing that the appropriate field strength necessary for maximum magnetic domain density in a Co/Pt multilayer depends on the thickness of the cobalt layers. By performing MFM microscopy on a sample with thicker (16Å) cobalt layers than the ones used for the preliminary study (8Å), we found that the magnetic domain density is maximized at a greater magnetic field magnitude than for thinner cobalt layers, in agreement with the associated increase of saturation field.

Keywords: Co/Pt thin films, MFM, VSM, domain topology, domain morphology, remanence, magnetization loop, magnetic domains

ACKNOWLEDGMENTS

I thank Dr. Karine Chesnel for her confidence, training, motivation, qualifications, and dedication to helping me succeed. I thank Berg Dodson for collaborating with Dr. Chesnel in order to train me quickly and efficiently; I also thank Berg for the work that he has done on other Co/Pt samples. I thank Phillip Salter, who designed the software used for the analysis of the MFM images. I finally express appreciation and thanks to my wife, without whom I wouldn't have been able to complete this project.

Table of Contents

Abstract	i
Acknowledgments.....	ii
Table of Contents	iii
Table of Figures	iv
1. Introduction.....	1
2. Methods.....	2
2.1 Overview	2
2.2 VSM Technique	3
2.3 MFM Technique	7
2.4 Magnetic Image Analysis	10
3. Results and Discussion	12
4. Conclusion	17
References.....	19

Table of Figures

Figure 1—PPMS and VSM Setup	4
Figure 2—Magnetization Loops	5
Figure 3— Magnetization Loops	5
Figure 4— Magnetization Loops	6
Figure 5— Magnetization Loops	6
Figure 6—AFM Diagram	8
Figure 7— $10 \times 10 \mu\text{m}^2$ AFM/MFM Image ($H_m = 2.00 \text{ T}$)	9
Figure 8—Black and White MFM Image	11
Figure 9— $[\text{Co}(16\text{\AA})/\text{Pt}(7\text{\AA})]_{50}$ Remanent MFM Images (H_m from 9 T to 0.8 T)	13
Figure 10— $[\text{Co}(16\text{\AA})/\text{Pt}(7\text{\AA})]_{50}$ Remanent MFM Images (H_m from 0.75 T to 0.3 T)	14
Figure 11— $[\text{Co}(16\text{\AA})/\text{Pt}(7\text{\AA})]_{50}$ Remanent MFM Images (H_m from 0.2 T to 0.1 T)	15
Figure 12—Magnetic Domain Density vs H_m	16
Figure 13—Magnetic Domain Density vs H_m (H_m from 4,500 Oe to 10,000 Oe).....	16

1. Introduction

The first commercial hard drive was introduced by IBM in 1956. The IBM 305 RAMAC had a storage capacity of 3.75 MB. Research in the field of data storage has evolved greatly since that time. For several years, the focus of the hard drive industry was a data writing method called longitudinal magnetic recording (LMR). In this method, the magnetization of data bits on a hard drive disk is parallel to the disk. The amount of data that can be stored via this method is greatly influenced by how large the magnetic domains that constitute the disk are (magnetic domain size affects how high the areal density of the disk is). These magnetic domains can store binary data. Research over the decades has resulted in a dramatic reduction in the size of these domains. This has allowed for an increase in the areal density of hard drive disks, and, consequently, great expansion in storage potential [1]. Researchers, however, eventually reached a point at which magnetic domain size could not be further reduced without running the risk of magnetic interference between domains (this is called the superparamagnetic effect or SPE), making the storage device unstable, especially at high temperatures [2]. When the method is used optimally, LMR can be used to store up to $100 \text{ GB}/\text{in}^2$, a density which is now considered limiting [3].

One solution to the SPE problem in data storage was to find an alternative data writing method. Perpendicular magnetic recording (PMR) is a data writing method in which the magnetization of the data bits that comprise a hard drive disk is perpendicular to the disk surface. Having the magnetization perpendicular to the disk instead of parallel provides the ability to store significantly more data bits (an estimated $1 \text{ TB}/\text{in}^2$ or higher) on the same physical size of hard disk [4]. In 2006, several major data storage companies (Western Digital, Seagate, Hitachi, and others) released hard drives that used PMR instead of LMR.

Research in materials that could further optimize the use of PMR in data storage has continued to this day. Multi-layer Co/Pt thin films exhibit perpendicular magnetic anisotropy, and are a promising material [5]. Perpendicular magnetic domains naturally form in this material, even in the absence of a magnetic field. The morphology of these domains at remanence, however, appears to depend on magnetic history. The morphology of these domains is of great interest in the data storage industry, for they determine the density of data bytes that could be stored. A study of Co/Pt thin films was undertaken by Dr. Karine Chesnel and some of her associates. Particularly, they focused on $[\text{Co}(8\text{\AA})/\text{Pt}(7\text{\AA})]_{50}$ (i.e. a Co/Pt multilayer thin film with 8 Å of cobalt layered on 7 Å of platinum 50 times) [6]. They found that magnetic domain density can be influenced when the material is previously magnetized to a critical level (somewhat before saturation). This measurement was carried at remanence (residual magnetism after the external magnetic field is brought back to zero). This report summarizes my efforts to contribute to the exploration of how the morphology and density of these magnetic domains depends on magnetic history (in this case, which fields have been applied before remanence) for a sample with thicker cobalt layers ($[\text{Co}(16\text{\AA})/\text{Pt}(7\text{\AA})]_{50}$).

2. Methods

2.1 Overview

A series of magnetization loops were applied perpendicularly to the $[\text{Co}(16\text{\AA})/\text{Pt}(7\text{\AA})]_{50}$ film using vibrating sample magnetometer (VSM) technique. Our VSM is part of a Quantum Design physical property measurement system (PPMS). After each magnetization loop was applied, a magnetic image was taken of the sample at remanence via magnetic force microscopy (MFM). These images provide information pertaining to the density and topology of the magnetic domains. A custom-

made program, called Magnetic Image Analyzer (MIA), enabled us to statistically analyze each of the MFM images.

2.2 VSM Technique

The PPMS instrument uses a superconducting magnet to produce a magnetic field of desired strength (up to 9 T). The superconducting magnet functions as follows: first, a power supply injects a current into the circuit; second, a persistent switch, which is a small portion of the superconducting magnet wire, gets heated by a resistive wire, causing the magnet controller to enter the superconducting circuit; third, a magnet controller drives the magnet to the current required for a higher magnetic field. The persistent switch heater is then turned off, and the process repeats itself until the desired magnetic field value is reached [7].

While a magnetization loop is being applied to a sample, the VSM enables us to track the magnetic moment M (see Figure 1). The VSM accesses the magnetic moment M by exploiting the Faraday effect, i.e. the fact that a changing magnetic flux will induce a voltage in a pickup coil:

$$V_{emf} = -\frac{\partial\Phi}{\partial t},$$

where V_{emf} is electromagnetic force and Φ is magnetic flux. As the name suggests, the vibrating sample magnetometer causes a sample to oscillate vertically near a pickup coil; this sinusoidal motion results in a changing magnetic flux and induced voltage. The voltage across the pickup coil is easily measured, and the following formula can be used to determine the magnetic moment of the sample:

$$M = \frac{V_{coil}}{2\pi f C A \sin(2\pi f t)},$$

where V_{coil} is voltage in the pickup coil, f is the frequency of oscillation (40 Hz), C is a coupling constant, A is the amplitude of oscillation (1–3 mm), and t is time [8]. Ultimately, we measure the magnetic moment M as a function of various parameters such as time t , temperature T , and magnetic field H . Our focus is primarily on magnetic moment as a function of magnetic field $M(H)$ throughout our magnetization loop measurements.



Figure 1—The PPMS and VSM setup. The VSM is located at position ①; samples are mounted through the top of the device and inserted inside the PPMS superconducting magnet, which is located at position ②. The pickup coils to perform VSM measurements are mounted before a sample is inserted. A CRYOMECH PT410 helium compressor is located at ③ to efficiently use the liquid helium needed for the superconducting components of the PPMS. A reservoir of liquid helium is located at ④.

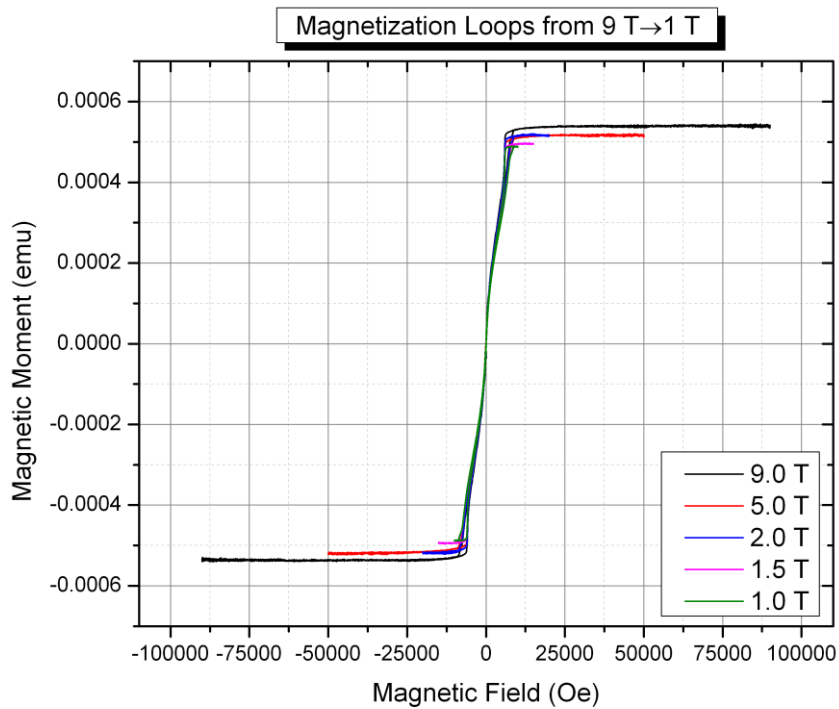


Figure 2—Magnetic moment of $[\text{Co}(16\text{\AA})/\text{Pt}(7\text{\AA})]_{50}$ as a function of magnetic field for the magnetization loops with a magnitude of 9.00 T, 5.00 T, 2.00 T, 1.50 T, and 1.00 T.

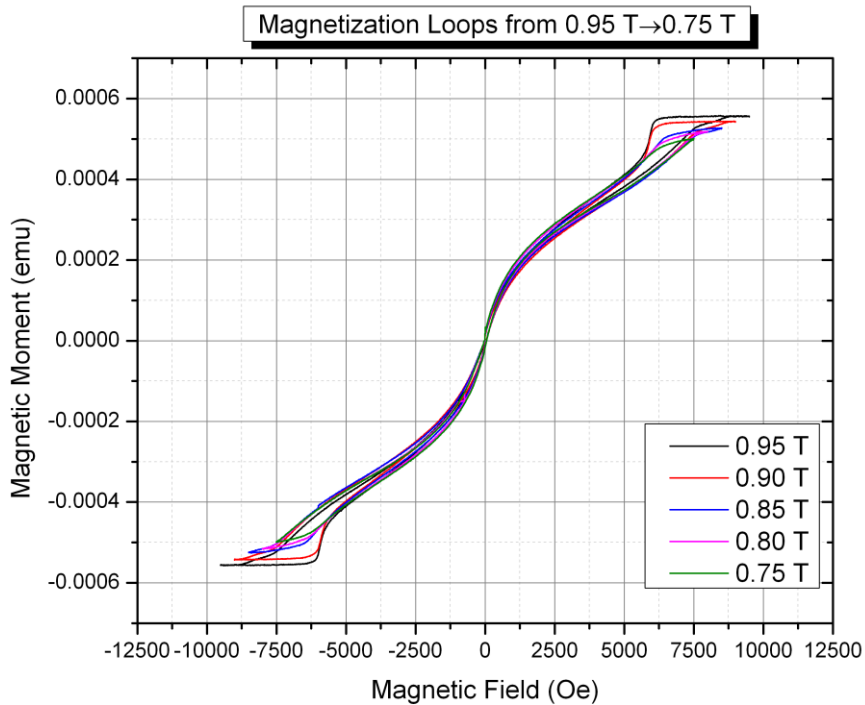


Figure 3—Magnetic moment of $[\text{Co}(16\text{\AA})/\text{Pt}(7\text{\AA})]_{50}$ as a function of magnetic field for the magnetization loops with a magnitude of 0.95 T, 0.90 T, 0.85 T, 0.80 T, and 0.75 T. The saturation field magnitude, $H_s = 0.85\text{ T}$, is apparent.

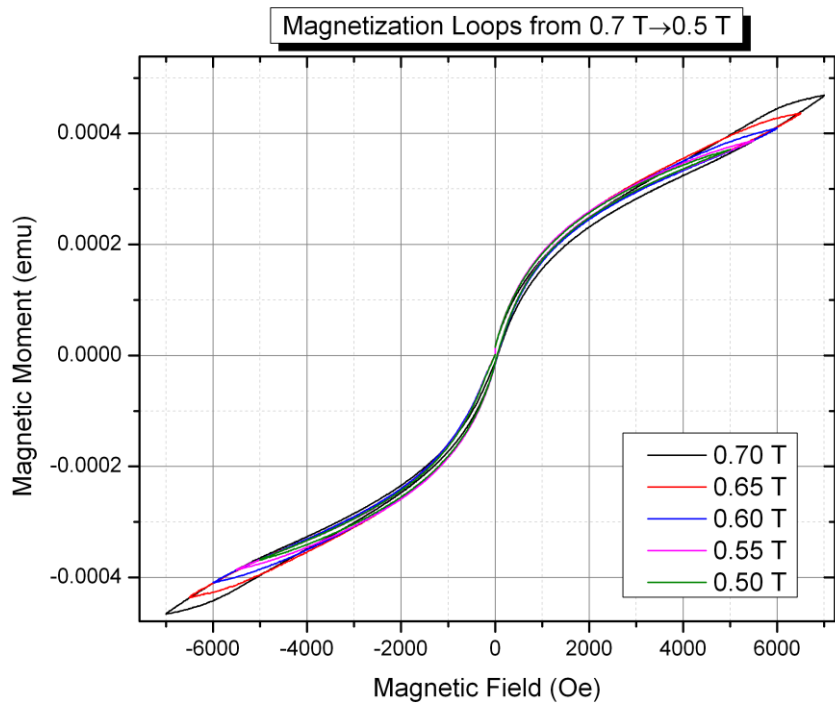


Figure 4—Magnetic moment of $[\text{Co}(16\text{\AA})/\text{Pt}(7\text{\AA})]_{50}$ as a function of magnetic field for the magnetization loops with a magnitude of 0.70 T, 0.65 T, 0.60 T, 0.55 T, and 0.50 T.

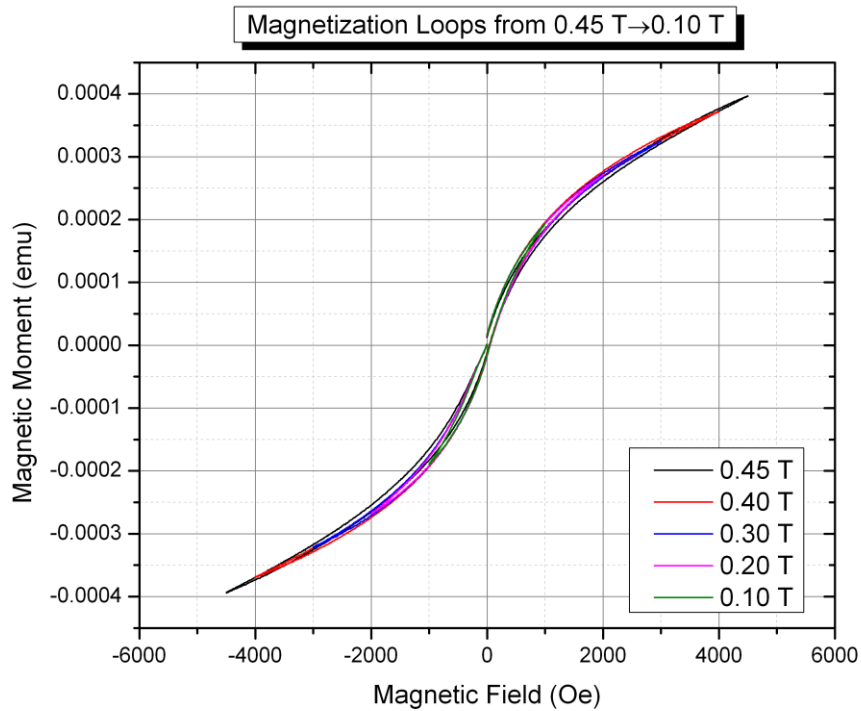


Figure 5—Magnetic moment of $[\text{Co}(16\text{\AA})/\text{Pt}(7\text{\AA})]_{50}$ as a function of magnetic field for the magnetization loops with a magnitude of 0.45 T, 0.40 T, 0.30 T, 0.20 T, and 0.10 T.

The $[\text{Co}(16\text{\AA})/\text{Pt}(7\text{\AA})]_{50}$ sample was kept at room temperature while the magnetization loops were applied to it during VSM measurements. My work focused on applying a series of magnetization loops with decreasing magnitude (a descending series). The first magnetization loop in the descending series had a magnetic field magnitude of 9.0 T (the sample was brought back down to remanence at the end of each magnetization loop). The last magnetic field applied to the sample had a magnitude of 0.1 T. Figures 2–5 show the magnetic moment of our sample as a function of magnetic field for each of the twenty magnetization loops that were applied to our sample throughout the course of the project.

2.3 MFM Technique

Magnetic force microscopy (MFM) is done simultaneously with atomic force microscopy (AFM). AFM is a scanning microscope in which a small tip at the end of a cantilever is moved across the surface of a sample, line by line, to generate an image of physical topography. This is possible because of the Van-der-Waals forces between the tip and the surface of the sample. These forces cause deflection in the cantilever attached to the tip. These deflections are measured by reflecting a laser beam off of the cantilever onto a position sensitive photodiode (PSPD); physical topography can be determined based on the readings of the PSPD (see Figure 6) [9]. We use tapping mode for our imaging, so the tip vibrates at its resonant frequency (typically 80–95 *kHz*) while moving across our samples line by line. Figure 7 (a) shows an example of an AFM image.

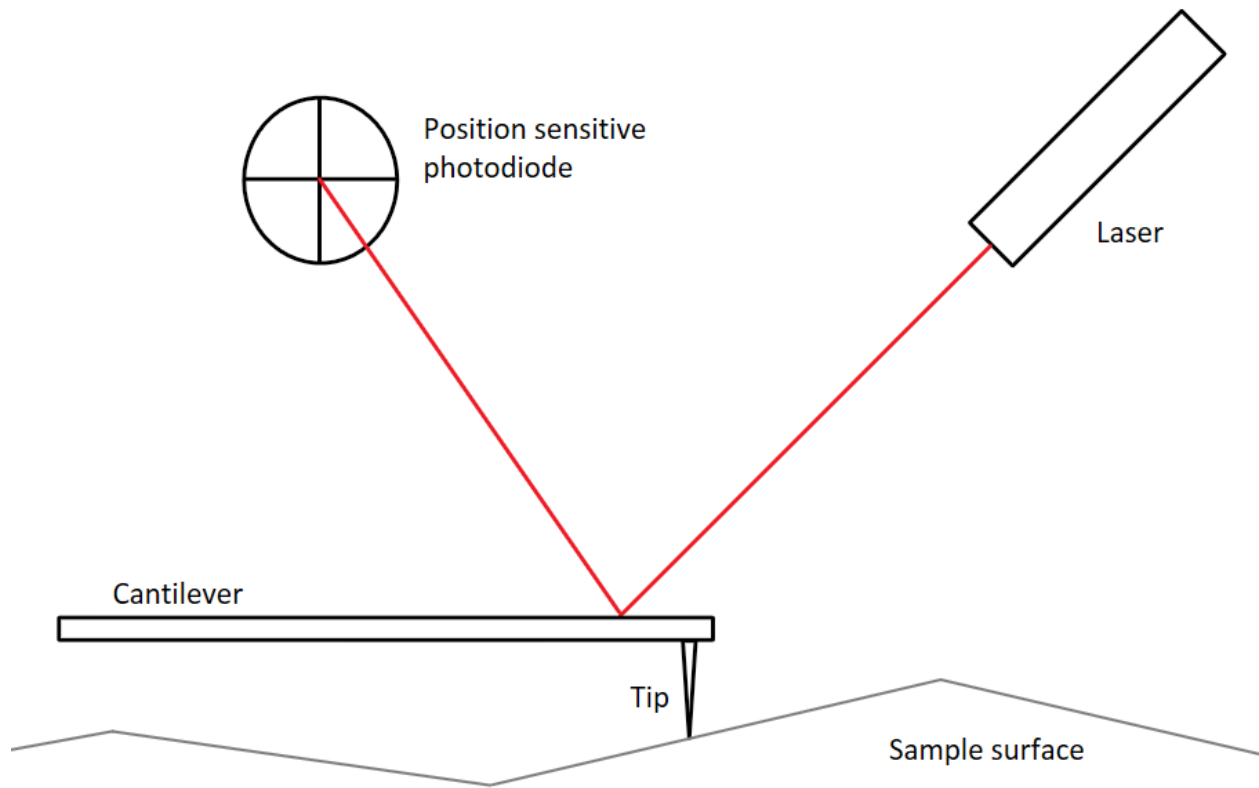


Figure 6—Basic diagram of how atomic force microscopy is performed. A laser beam is reflected off of the top of the cantilever onto a PSPD. As the tip moves across the sample surface, the atomic force between the sample and the tip cause the cantilever to deflect, which moves the laser to a different position on the PSPD. The PSPD readings are used to map out the topography of the sample.

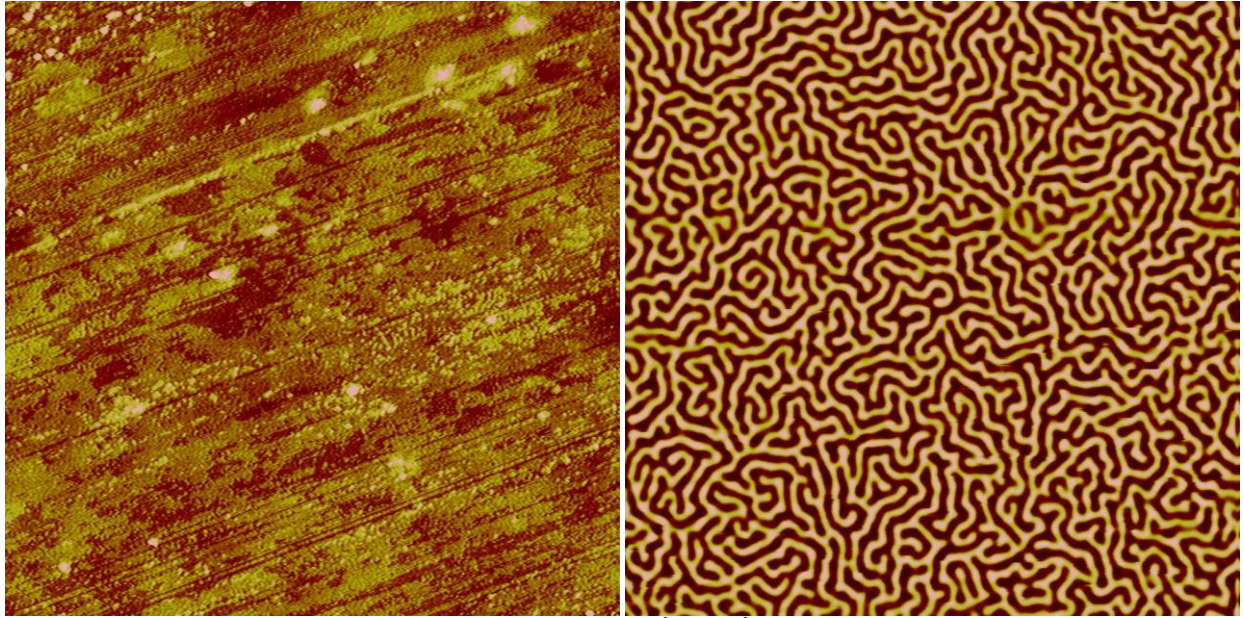


Figure 7—(a) A $10 \times 10 \mu m^2$ AFM image of $[Co(16\text{\AA})/Pt(7\text{\AA})]_{50}$. (b) A $10 \times 10 \mu m^2$ MFM image of $[Co(16\text{\AA})/Pt(7\text{\AA})]_{50}$ taken at remanence after a magnetization loop with a magnitude of 2.0 T was applied ($H_m = 2.0 T$).

For MFM to be performed, the tip mounted on a cantilever must first be magnetized. After an AFM line is recorded, the microscope head is lifted to a height, typically 40–70 nm, above the sample. Once lifted, the tip is moved across the sample again on the same line, retracing the topography that was just measured via AFM. If the material being scanned exhibits perpendicular magnetic stray fields, the tip will be deflected via magnetic interaction with the sample. This deflection causes a phase difference between the path recorded during the AFM line and the path recorded during the MFM line. This phase difference is recorded on the PSPD, which determines whether the tip was attracted to the sample or repelled away from the sample for all points along the line. This information yields an image of the magnetic domains present in the sample [10]. Figure 7 (b) displays an example of a MFM image. Magnetic domains, areas of the sample that are magnetized in the same direction, are indicated on the MFM image by regions of the same color (either yellow or brown): the brown signifies magnetization opposite the previously applied

field, while the yellow signifies magnetization aligned with the previously applied field. If the sample were saturated, not at remanence, then no domains would remain, and a MFM image would appear purely yellow.

A $10 \times 10 \mu\text{m}^2$ MFM image was taken of our $[\text{Co}(16\text{\AA})/\text{Pt}(7\text{\AA})]_{50}$ sample after each of the twenty magnetization loops were applied. These images hold information pertaining to the morphology and density of magnetic domains of our Co/Pt samples.

2.4 Magnetic Image Analysis

The MIA program allows us to determine the number of each type of magnetic domains that are present in our MFM images (pointing out of or into the sample), and, thus, the density of magnetic domains throughout our sample (for each of the magnetization loops applied). The program also computes the size of each magnetic domain in our images, the average domain size throughout the sample, and the net magnetization of our sample. Without such a program, quantitative analysis of our MFM images would be nearly impossible. The MIA accomplishes all this through four simple steps:

1. *Binary rendering of the MFM image (see Figure 8)*—while the program is running, the user is prompted to enter a cutoff value between 0 and 250 (0 corresponds to all white and 250 corresponds to all black). All pixels in the image that have a value lower than the cutoff entered by the user are converted into white pixels (up or +), while those with a value higher than the one entered are converted into black pixels (down or -).

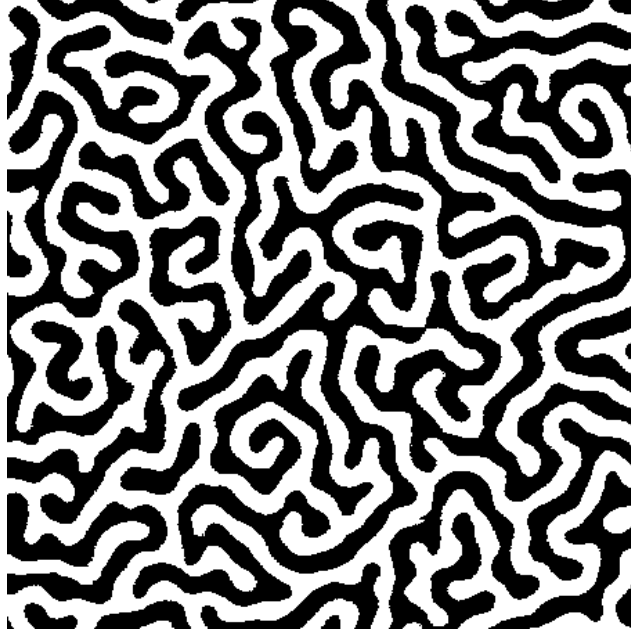


Figure 8—A portion of the MFM image displayed in Figure 7 that has been rendered black and white by the MIA program. White represents upward pointing magnetic domains; black represents downward pointing magnetic domains.

2. *Listing the domains*—the program scans the image from right to left and top to bottom, counting the clusters of pixels that are surrounded by pixels of the opposite color. The domains are listed along with their sizes (in pixels).
3. *Counting the domains*—from the list of domains and sizes, the program counts the total number of domains pointing up and down (D_+ and D_- , respectively), the total number of up and down pixels (N_+ and N_- , respectively), and the average domain area (S_+ and S_-).

$$S_+ = \frac{N_+}{D_+} \text{ and } S_- = \frac{N_-}{D_-}.$$

4. *Calculating net magnetization*—based on the information found in step three, the program determines a normalized net magnetization of the sample, M , through the following equation:

$$M = \frac{N_+ - N_-}{N_+ + N_-}.$$

M is normalized such that $-1 \leq M \leq 1$: $M = -1$ when $N_+ = 0$, and $M = 1$ when $N_- = 0$. The user-input value described in step one is chosen such that the net magnetization calculated in step four matches that of the sample after the applied magnetization loop as experimentally measured. As can be seen in Figures 2–5, after each magnetization loop is applied, the net magnetic moment of $[\text{Co}(16\text{\AA})/\text{Pt}(7\text{\AA})]_{50}$ is slightly above zero once remanence is reached $M \cong 0$.

3. Results and Discussion

As indicated in Figure 3, the saturation field magnitude for $[\text{Co}(16\text{\AA})/\text{Pt}(7\text{\AA})]_{50}$ is $H_s = 0.85 \text{ T}$, which is higher than that of $[\text{Co}(8\text{\AA})/\text{Pt}(7\text{\AA})]_{50}$ ($H_s = 0.60 \text{ T}$) [6]. This leads us to anticipate that the magnetic field magnitude, H^* , necessary to maximize the magnetic domain density of $[\text{Co}(16\text{\AA})/\text{Pt}(7\text{\AA})]_{50}$ is also greater than that of $[\text{Co}(8\text{\AA})/\text{Pt}(7\text{\AA})]_{50}$ ($H^* = 0.5 \text{ T}$). MFM images corresponding to each of the twenty applied magnetization loops applied to $[\text{Co}(16\text{\AA})/\text{Pt}(7\text{\AA})]_{50}$ are displayed below in Figures 9–11 (note that H_m is the magnitude of the field previously applied).

[Co(16Å)/Pt(7Å)]₅₀ Remanent MFM Images

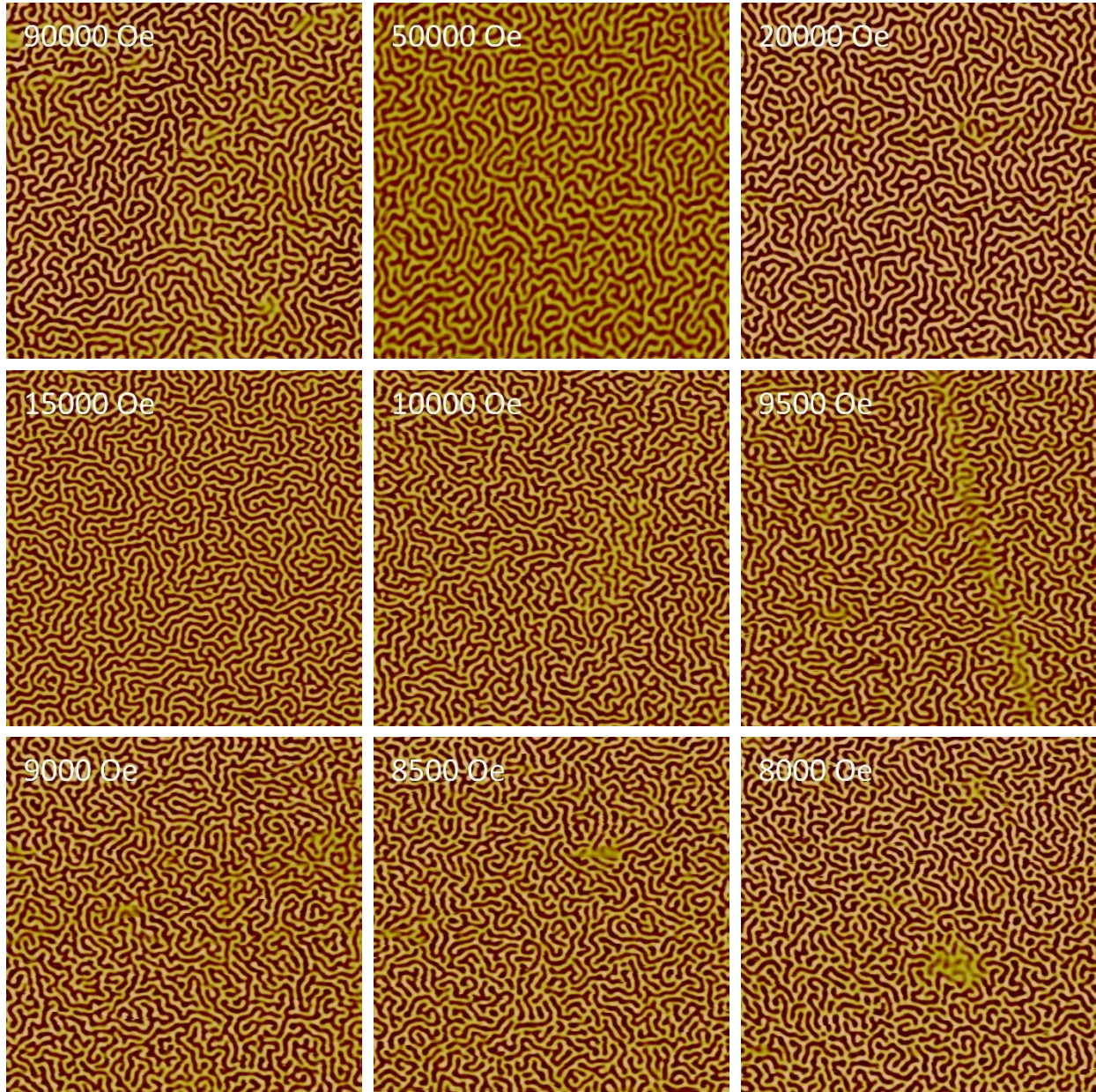


Figure 9— $10 \times 10 \mu m^2$ MFM images of [Co(16Å)/Pt(7Å)]₅₀ taken at remanence for indicated H_m from 9 T–0.8 T

[Co(16Å)/Pt(7Å)]₅₀ Remanent MFM Images

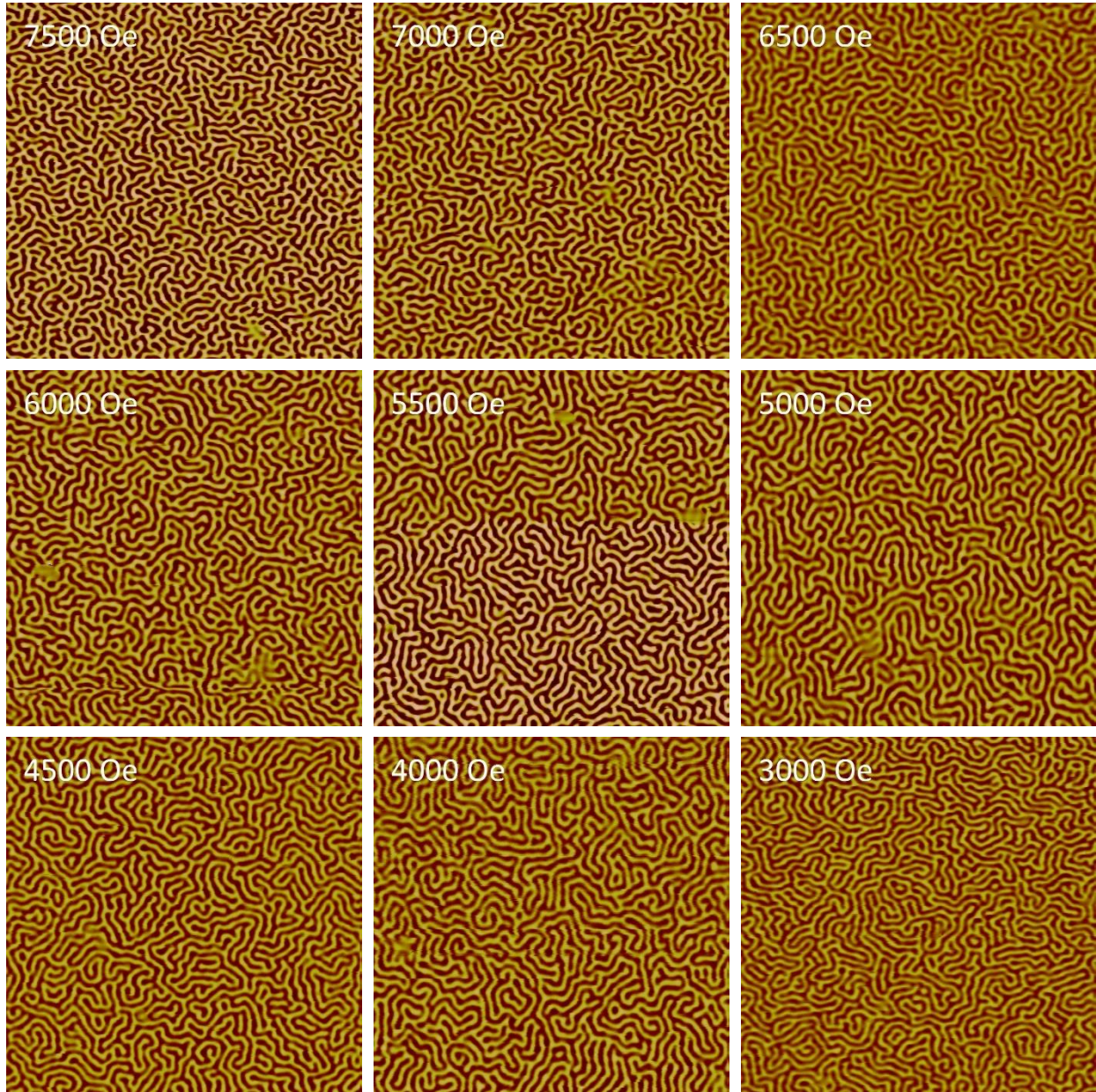


Figure 10— $10 \times 10 \mu m^2$ MFM images of [Co(16Å)/Pt(7Å)]₅₀ taken at remanence for indicated H_m from 0.75 T–0.3 T

[Co(16Å)/Pt(7Å)]₅₀ Remanent MFM Images

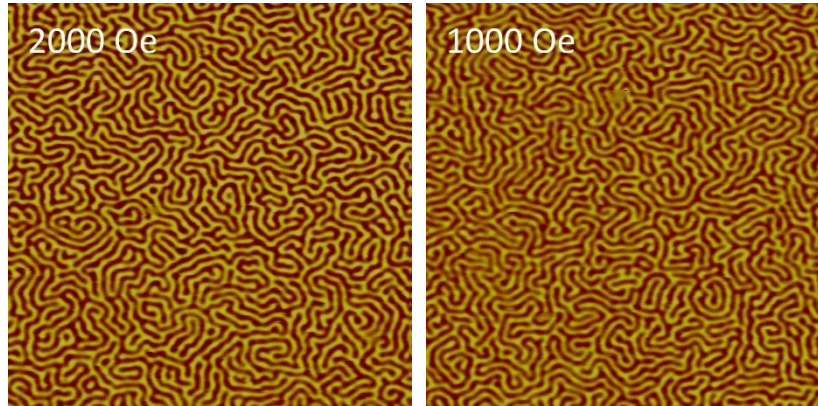


Figure 11— $10 \times 10 \mu\text{m}^2$ MFM images of [Co(16Å)/Pt(7Å)]₅₀ taken at remanence for indicated H_m from 0.2 T–0.1 T

In the first few MFM images, both the downward pointing and upward pointing magnetic domains take on a maze-like structure (Figure 9, H_m from 9 T–0.9 T). As the magnitude of the magnetization loops applied becomes lower than the value necessary to saturate [Co(16Å)/Pt(7Å)]₅₀, the downward pointing domains (the dark domains) begin to shrink in length. This occurs because, since the sample does not get fully saturated, the domains that oppose the direction of the applied magnetic field do not entirely collapse once the magnetic field reaches its highest value H_m ; their presence prevents the magnetic domains that form while the magnetic field approaches remanence from becoming long and maze-like [6]. The result is a greater density of smaller magnetic domains for several magnetization loops (Figure 9 and Figure 10, H_m from 0.85 T–0.65 T). As the magnitude of H_m decreases further below that point, the density of downward-pointing magnetic domains decreases, and the dark domains extend in length and return to a maze-like structure (Figures 9–11, H_m from 0.6 T–0.1 T).

Although difficult to detect with the naked eye on the MFM image, the density of downward pointing magnetic domains in [Co(16Å)/Pt(7Å)]₅₀ clearly reaches a peak at an optimizing field magnitude in the descending series of magnetization loops. Figure 12 and Figure 13 show plots of

the number of both types of magnetic domains as a function of the maximum magnetic field H_m of the previously applied magnetization loop.

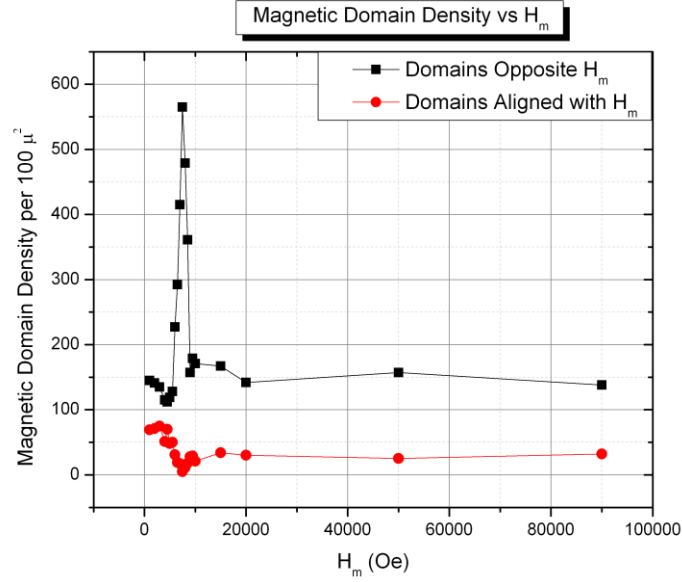


Figure 12—Plot of the number of upward and downward pointing magnetic domains per $100 \mu m^2$ as a function of the magnitude of the previously applied magnetization loop (H_m).

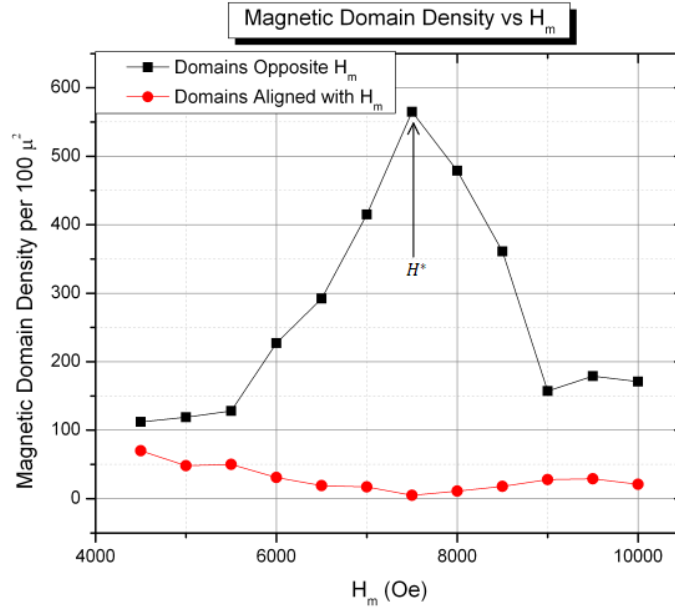


Figure 13—Zoom of Figure 12, displaying the 4,500–10,000 Oe region.

As was the case for $[\text{Co}(8\text{\AA})/\text{Pt}(7\text{\AA})]_{50}$, the magnetic domain density of $[\text{Co}(16\text{\AA})/\text{Pt}(7\text{\AA})]_{50}$ can be optimized by adjusting the previously applied magnetic field. The magnetic domain density of

[Co(16Å)/Pt(7Å)]₅₀ was maximized to above 550 domains/100 μm², nearly five times the initial domain density, after a magnetization loop with a magnitude of $H_m = H^* = 7,500 Oe$ was applied to the sample (for [Co(8Å)/Pt(7Å)]₅₀, it was maximized at $H^* = 5,000 Oe$). For both [Co(8Å)/Pt(7Å)]₅₀ and [Co(8Å)/Pt(7Å)]₅₀, H^* is somewhat lower than the respective saturation field H_s ($H^* < H_s$). The maximum density of downward pointing magnetic domains that were found in [Co(16Å)/Pt(7Å)]₅₀ was ~565 per 100 μm² (compared with ~600 per 100 μm² for [Co(8Å)/Pt(7Å)]₅₀) [6].

4. Conclusion

Remanent magnetic domain density for [Co(16Å)/Pt(7Å)]₅₀ is maximized at a field magnitude of $H^* = 7,500 Oe$. This field strength is greater than that of [Co(8Å)/Pt(7Å)]₅₀ in agreement with the increase in saturation field H_s . We thus conclude that the magnitude of the magnetization loop that is needed to maximize magnetic domain density in a Co/Pt multilayer sample seems to increase with the thickness of the cobalt layers in the material. Research is currently underway with samples that have 4 Å, 12 Å, 25 Å, 31 Å, 40 Å, and 60 Å thick cobalt layers. Once we determine at which magnetic field magnitudes these samples exhibit a maximum density of magnetic domains, we will be in a position to map out the relationship between the thickness of cobalt layers and the magnetic field necessary to maximize the density of magnetic domains in Co/Pt multilayers.

The measured maximum density of downward pointing magnetic domains attained at the optimizing magnetization loop for [Co(16Å)/Pt(7Å)]₅₀ was approximately 565 per 100 μm². This number could possibly be further increased by using higher resolution around the peak for the 16Å sample. In the future we will revisit [Co(16Å)/Pt(7Å)]₅₀ and apply fields from 8,000 *Oe* to 7,000 *Oe* at intervals of 100 *Oe*, analyzing the density of downward pointing magnetic domains.

This will help us determine whether cobalt layer thickness also correlates with the maximum density of downward pointing magnetic domains in addition to peak location.

References

- [1] Perpendicular *magnetic recording (PMR)*. Lake Forest, CA: Western Digital Technologies (2006).
- [2] Kryder, M. H. Magnetic recording beyond the superparamagnetic limit. *2000 IEEE International*, **1**, 575 (2000).
- [3] Weller, D., & Doerner, M. F. Extremely high-density longitudinal magnetic recording media. *Annual Review of Materials Science*, **30**, 611 (2000).
doi:10.1146/annurev.matsci.30.1.611
- [4] Khizroev, S. In Dmitri Litvinov, SpringerLink (Online service) and by Sakhrat Khizroev D. L. (Eds.), *Perpendicular magnetic recording* Springer Netherlands, Dordrecht (2005).
- [5] Hwang, P., Li, B., Yant, T., & Zhu, F. Perpendicular magnetic anisotropy of Co₈₅Cr₁₅/Pt multilayers. *Journal of University of Science and Technology Beijing*, **11**(4), 319-323 (2004).
- [6] Westover, A., Chesnel, K., Hatch, K., Salter, P., & Hellwig, O. Enhancement of magnetic domain topologies in Co/Pt thin film by fine tuning magnetic field path throughout hysteresis loop. *Journal of Magnetism and Magnetic Materials*, **399**, 164 (2016).
doi:10.1016/j.jmmm.2015.09.040
- [7] *Physical property measurement system hardware manual*, 6th ed. (Quantum Design, San Diego, CA) 45 (2008).
- [8] *Vibrating sample magnetometer (VSM) option User's manual*, 5th ed. (Quantum Design, San Diego, CA) 18 (2011).
- [9] *Atomic force microscopy (AFM)*, In H. Yang (Eds.), (Nova Science Publishers, Inc., Hauppauge, NY) 57 (2014).
- [10] Ferri, F. A., Pereira, M. A., & Marega Jr., E. Magnetic force microscopy: Basic principles and applications. In V. Bellitto (Ed.), *Atomic force microscopy - imaging, measuring and manipulating surfaces at the atomic scale* (Rijeka, Croatia: InTech) 39 (2012).